JMEPEG (2011) 20:1591–1599
DOI: 10.1007/s11665-010-9813-z

1059-9495/$19.00

Effects of Cross-Sectional Ovalization on Springback and Strain Distribution of Circular Tubes Under Bending

Yafei Liu and Daxin E

(Submitted November 19, 2009; in revised form November 8, 2010)

Springback and cross-sectional ovalization are two important defects in the bending formation of tubular parts. In this article, an analytic model considering ovalization is presented to calculate the springback and tangential strain in tube bending. Compared with the calculation neglecting ovalization, the proposed model could better predict the trends of springback angle over bending radius ratio and wall thickness ratio. Moreover, calculation of the tangential strain indicates that the bending deformation is more severe in the middle than at the ends of a bent tube. Through comparison of the results of this model and the calculations neglecting ovalization, it is shown that the effects of ovalization on springback are negligible only if the bending radius ratio and the wall thickness ratio are large enough. Also, the influence of ovalization differs a lot from one material to another.

Keywords aluminum, shaping, springback, stainless steel, tube bending

1. Introduction

Bending forming is widely utilized to produce tubular parts in automotive, aerospace, and oil industries. The tube bending technology has long been limited by a series of forming defects, including bending springback, cross-sectional distortion, wall thickness variation, and wrinkling. Bending springback is the change in bending angle resulting from the elastic strain recovery during unloading. The distortion of the cross section, which takes the form of ovalization in the case of a circular tube (Ref 1), is an unwanted byproduct of the bending process (Ref 2). It changes the interior shape of the bent tube and thus influences the tube's performance in fluid transmission. Cross-sectional distortion also influences the bending springback of a beam (Ref 3-5). The laws of cross-sectional distortion have been investigated and several approaches have been proposed to control the distortion (e.g., Ref 1, 6-12).

The accurate prediction of tube bending springback has been a challenging task. A number of analytic models have been presented successively to calculate the springback. Al-Qureshi (Ref 13, 14) analyzed circular tube bending assuming that the material is ideally plastic and calculated the change in curvature radius caused by springback. This model was further developed by Megharbel et al. (Ref 15) by taking strain hardening into account. As the accuracy of elbow angle is crucial in the manufacturing and assembly of pipelines, the springback angle has also been paid attention to Zhan et al. (Ref 16) investigated the dependence of springback angle on bending angle and material parameters. More recently, Daxin and Liu (Ref 17) predicted the springback angle of 1Cr18Ni9Ti stainless steel tubes and addressed the relations between springback angle and geometrical parameters. This review is not exhaustive; many experimental and numerical investigations on springback

Yafei Liu and **Daxin E**, School of Materials Science and Engineering, Beijing Institute of Technology, Beijing 100081, China. Contact e-mails: yafei.liu@mail.utexas.edu and daxine@bit.edu.cn.

Nomenclature

R	bending radius (curvature radius of neutral surface before unloading)
R'	curvature radius of neutral surface after unloading
d	outer diameter
r	outer radius
t	wall thickness
R/d	bending radius ratio
t/d	wall thickness ratio
φ	bending angle (angle before unloading)
φ'	angle after unloading
$\Delta\varphi$	springback angle
θ	tangential position on the bent tube
α_1, α_2	circumferential positions on the cross sections of the tube
ρ	curvature radius before unloading
ρ'	curvature radius after unloading
a	length of the major axis of the distorted cross section
b	length of the minor axis of the distorted cross section
E	Young's modulus
C	strength coefficient
n	strain hardening exponent
ε	tangential strain
σ	tangential stress
ε_{max}	maximum tangential strain (tangential strain at the extrados)
D	calculation deviation rate of springback angle
B	breadth of the cross section
I	cross-sectional moment of inertia
M	bending moment
UDR	uniformly distorted region
NUDR	non-uniformly distorted region

prediction and compensation have also been reported in recent years.

Despite the insights gained, our previous model (Ref 17) has limitations because the bending deformation of a tube is complicated and several assumptions had to be adopted to simplify the analysis. The cross section was considered unchanged during bending. For the material (1Cr18Ni9Ti steel) and processing parameters discussed, the ovalization is not significant so that the prediction basically agree with experiments after being corrected. Nevertheless, bending with larger ovality was not addressed and the effects of ovalization are not known. Moreover, the wall thickness was assumed to be small compared with the tube diameter, making the analysis less accurate when the wall thickness is thicker.

This article presents an improved model for tube bending analysis. The wall thickness is no longer assumed to be very small. More importantly, the cross-sectional ovalization is taken into account in the analysis. The non-uniformity of cross-sectional distortion in practical bending processes is also considered. Furthermore, aluminum tubes (5A03) and small bending radius ratios ($R/d = 2$), both of which render relatively severe ovalization, are studied experimentally and analytically. Based on the newly proposed model, the bending springback angle is predicted, and the results are compared with both experiments and the calculations neglecting ovalization. The strain distribution alongside the tubes is also explored. The effects of ovalization on springback and strain distribution are discussed.

2. Analysis Neglecting Ovalization

The geometry of a bent tube is shown in Fig. 1. The tangential length of the neutral surface is considered the same before and after unloading (Ref 17). Thus,

$$R\varphi = R'\varphi' \quad \text{(Eq 1)}$$

where R is the curvature radius before unloading, or the bending radius; and R' is the curvature radius after unloading; φ is the angle before unloading, or the bending angle; and φ' is the angle after unloading.

Based on the plane's cross section assumption, for arbitrary fiber layer in the tube wall, there is an equation (Ref 17)

$$\frac{y}{R} - \frac{y}{R'} = \frac{My}{EI} \quad \text{(Eq 2)}$$

where M is the bending moment, I the cross-sectional moment of inertia, and E the Young's modulus of the material.

Based on Eq 1 and 2, the expression of springback angle is obtained:

$$\Delta\varphi = \varphi - \varphi' = \frac{MR}{EI}\varphi \quad \text{(Eq 3)}$$

As the cross section of a circular tube is symmetric about the neutral axis, the bending moment could be calculated as (Ref 15)

$$\begin{aligned} M &= 2\int_0^r y\cdot\sigma B(y)dy \\ &= 2\left\{\int_0^{r-t} y\cdot C\left(\frac{y}{R}\right)^n\cdot 2\left[\sqrt{r^2-y^2}-\sqrt{(r-t)^2-y^2}\right]dy \right. \\ &\quad \left. + \int_{r-t}^{r} y\cdot C\left(\frac{y}{R}\right)^n\cdot 2\sqrt{r^2-y^2}dy\right\} \end{aligned} \quad \text{(Eq 4)}$$

where r and t are the outer radius and wall thickness of the tube, respectively; C and n are the strength coefficient and strain hardening exponent of the material, respectively. In this expression, a power-law stress-strain relation is adopted.

The cross-sectional moment of inertia is expressed as

$$I = \frac{\pi}{4}\left[r^4 - (r-t)^4\right] \quad \text{(Eq 5)}$$

Substituting Eq 4 and 5 into Eq 3, we obtain

$$\Delta\varphi = \frac{16CR^{1-n}\left\{\int_0^r y^{n+1}\sqrt{r^2-y^2}dy - \int_0^{r-t} y^{n+1}\sqrt{(r-t)^2-y^2}dy\right\}}{\pi E\left[r^4-(r-t)^4\right]}\varphi \quad \text{(Eq 6)}$$

Given that $\sin\alpha_1 = y/r$, and $\sin\alpha_2 = y/(r-t)$, this equation becomes

$$\Delta\varphi = \frac{16\eta CR^{1-n}\varphi}{\pi E}\cdot\frac{\left[r^{n+3}-(r-t)^{n+3}\right]}{\left[r^4-(r-t)^4\right]} \quad \text{(Eq 7)}$$

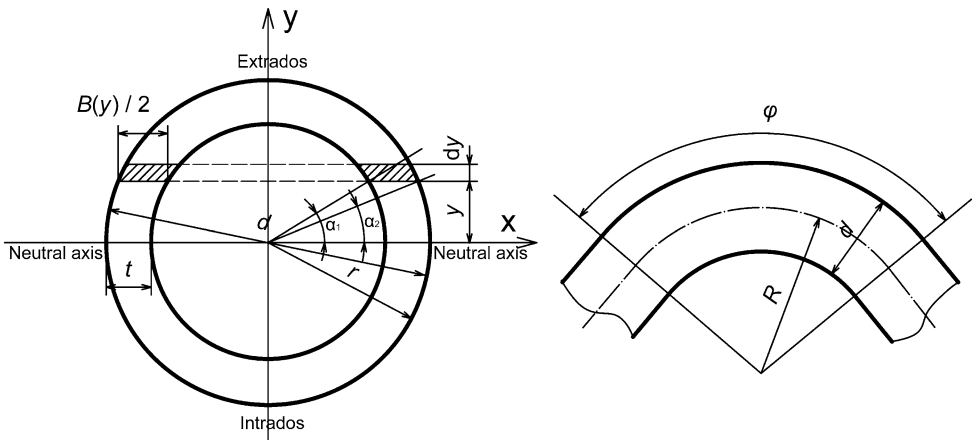

Fig. 1 Geometry of a bent tube without cross-sectional distortion

where

$$\eta = \int_0^{\frac{\pi}{2}} \left(\sin^{n+1}\alpha - \sin^{n+3}\alpha\right) d\alpha \qquad \text{(Eq 8)}$$

Clearly, the value of η is determined by the strain hardening exponent alone.

The maximum tangential strain, namely, the tangential strain at the extrados, could be given as

$$\varepsilon_{\max} = \frac{r}{R} \qquad \text{(Eq 9)}$$

3. Analysis Considering Ovalization

In the elastic-plastic bending of tubes, a major part of the cross section has been plastically distorted at the end of loading. Thus, substituting the original dimensions of the cross section into Eq 7 and 9 will not yield the precise calculation results of springback angle and tangential strain. An approach with greater accuracy is to consider the shape and dimensions of the distorted cross section in the calculation.

To begin with, consider an idealized case in which the shape and dimensions of the distorted cross section are the same along the length of a bent tube. Experiments have shown that the external and internal contours of a distorted cross section could be closely approximated by two ellipses when the ovalization is not too severe (see Fig. 2a). Thus, the outer contour of the distorted cross section could be approximately given as

$$\frac{x^2}{a^2} + \frac{y^2}{b^2} = 1 \qquad \text{(Eq 10)}$$

where a and b are the lengths of the major and minor axes of the ellipse, respectively. The inner contour of could be given as

$$\frac{x^2}{(a-t)^2} + \frac{y^2}{(b-t)^2} = 1 \qquad \text{(Eq 11)}$$

where t is the wall thickness of the tube. The geometry of the distorted cross section is shown in Fig. 2(b).

The breadth of the cross section at the distance y from the neutral axis is given as

$$B(y) = 2\left[a\sqrt{1-\frac{y^2}{b^2}} - (a-t)\sqrt{1-\frac{y^2}{(b-t)^2}}\right] \qquad \text{(Eq 12)}$$

when $y < b - t$ or

$$B(y) = 2a\sqrt{1-\frac{y^2}{b^2}} \qquad \text{(Eq 13)}$$

when $b - t < y < b$.

Similar Eq 4, the bending moment could be expressed as

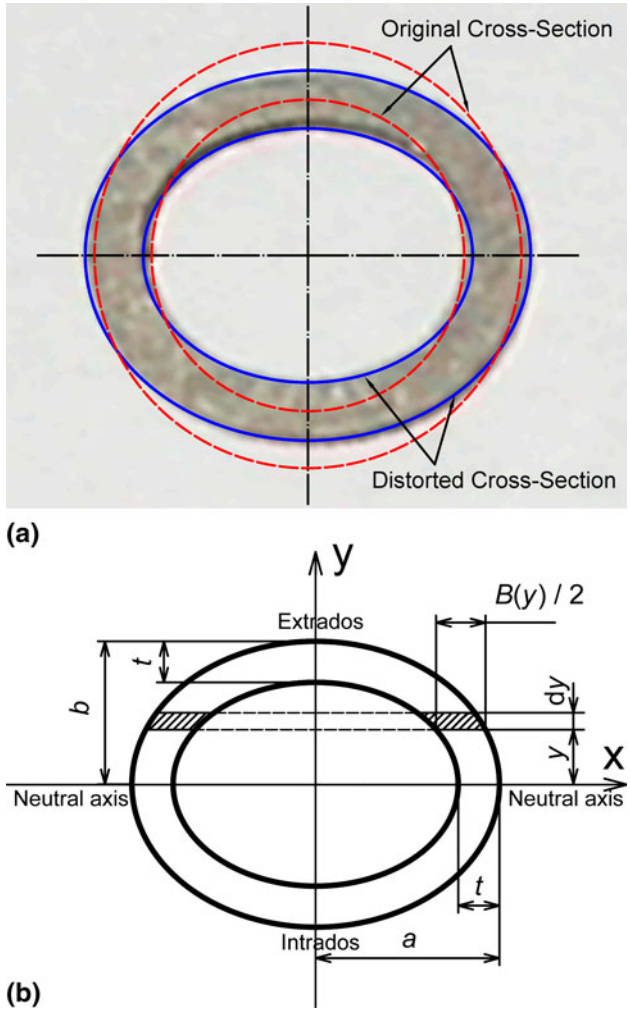

Fig. 2 Cross section after bending deformation. (a) Photograph of a distorted cross section. The bent tube was cut utilizing a wire cutting machine. (b) Geometry of an elliptical cross section

$$\begin{aligned} M &= 2\int_0^b y\cdot\sigma B(y)dy \\ &= 2\left\{\int_0^{b-t} y\cdot C\left(\frac{y}{R}\right)^n\cdot 2\left[a\sqrt{1-\frac{y^2}{b^2}} - (a-t)\sqrt{1-\frac{y^2}{(b-t)^2}}\right]dy\right. \\ &\quad \left. + \int_{b-t}^{b} y\cdot C\left(\frac{y}{R}\right)^n\cdot 2a\sqrt{1-\frac{y^2}{b^2}}dy\right\} \end{aligned} \qquad \text{(Eq 14)}$$

The cross-sectional moment of inertia of the distorted cross section is

$$I(\theta) = \frac{\pi}{4}\left[ab^3 - (a-t)(b-t)^3\right] \qquad \text{(Eq 15)}$$

Substituting Eq 14 and 15 into Eq 3, we obtain

$$\Delta\varphi = \frac{16CR^{1-n}\left\{\int_0^{b-t} y^{n+1}\cdot\left[a\sqrt{1-\frac{y^2}{b^2}} - (a-t)\sqrt{1-\frac{y^2}{(b-t)^2}}\right]dy + \int_{b-t}^{b} y^{n+1}\cdot a\sqrt{1-\frac{y^2}{b^2}}dy\right\}}{\pi E\left[ab^3 - (a-t)(b-t)^3\right]}\varphi \qquad \text{(Eq 16)}$$

Given that $\sin\beta_1 = y/b$, and $\sin\beta_2 = y/(b-t)$, this equation becomes

$$\Delta\varphi = \frac{16CR^{1-n}\varphi\left\{ab^{n+2}\int_0^{\frac{\pi}{2}}\left(\sin\beta_1^{n+1} - \sin\beta_1^{n+3}\right)d\beta_1 - (a-t)(b-t)^{n+2}\int_0^{\frac{\pi}{2}}\left(\sin\beta_2^{n+1} - \sin\beta_2^{n+3}\right)d\beta_2\right\}}{\pi E\left[ab^3 - (a-t)(b-t)^3\right]}$$
$$= \frac{16\eta CR^{1-n}\varphi}{\pi E}\cdot\frac{\left[ab^{n+2} - (a-t)(b-t)^{n+2}\right]}{\left[ab^3 - (a-t)(b-t)^3\right]} \quad \text{(Eq 17)}$$

The expression of η has been given in Eq 8.

The maximum tangential strain, namely the tangential strain at $y = b$, could be given as

$$\varepsilon_{\max} = \frac{b}{R} \quad \text{(Eq 18)}$$

The analytic solution of springback angle and maximum tangential strain considering ovalization could be easily obtained by substituting the analytic expressions of a and b into Eq 17 and 18. In this way, springback angle and maximum tangential strain could be expressed as functions of geometric parameters and material parameters. However, in order to reveal the effects of ovalization in a more precise way, the measured dimensions of the distorted cross section will be utilized instead.

In practical bending processes, the ovalization is not uniform in the longitudinal direction. Schematically, Fig. 3 shows the geometry of a bent tube with non-uniform ovalization. The tube could be divided into three regions. They will be referred to as the uniformly distorted region (UDR), the non-uniformly distorted region (NUDR) and the undeformed region. The two ends of the deformed region are constrained by the undeformed region. The forces applied by the clamps and/or insert plugs (Ref 1) at the ends also lead to the traverse deformation of the cross section. As a result, a non-uniformly distorted region is produced at the ends of the deformed region. But in the middle region far away from the undeformed region, the effects of the transverse constrain are negligible according to the Saint-Venant's principle. Thus, the bending moment acts as the only load and the ovalization is supposed to be uniform. This region is the UDR. As a matter of fact, both the experiments performed by Khodayari (Ref 18) and the bending tests in this study have verified that the ovalization in the UDR is basically uniform and larger than that in the NUDR.

Consider the cross section at arbitrary tangential position of a non-uniformly distorted tube. The expression of the bending moment could be written as

$$M = 2\int_0^b y[C\varepsilon^n(y)]B(y)dy \quad \text{(Eq 19)}$$

in which

$$\varepsilon(y) = \varepsilon_{\max}\frac{y}{b} \quad \text{(Eq 20)}$$

where $\varepsilon_{\max}$ is the tangential strain at the extrados.

Equations 19 and 20 yield

$$\varepsilon_{\max} = b\left(\frac{M}{2C\int_0^b y^{n+1}B(y)dy}\right)^{1/n} \quad \text{(Eq 21)}$$

We can further obtain

$$\rho = \frac{b}{\varepsilon_{\max}} = \left(\frac{M}{2C\int_0^b y^{n+1}B(y)dy}\right)^{-\frac{1}{n}} \quad \text{(Eq 22)}$$

where ρ is the curvature radius of the neutral surface at the same tangential position.

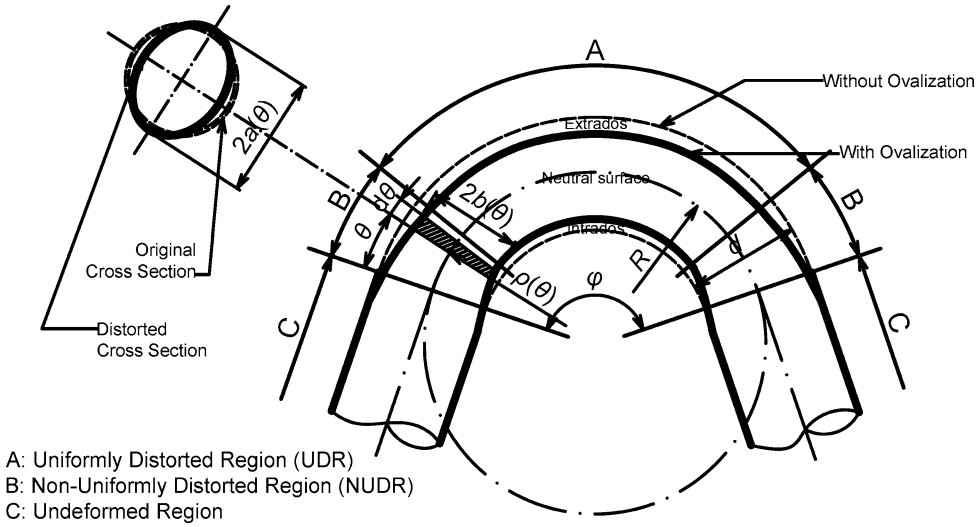

Fig. 3 Schematic of a bent tube with non-uniform ovalization

Since the bending moment is considered constant along the tube, the more oval the distorted cross section, the smaller the integral in Eq 22 and the smaller the curvature radius. Therefore, the curvature radius in the UDR is smaller than that in the NUDR. Also, the curvature radius is almost uniform in the UDR. The bending tests in this study showed that the region $\varphi/4 < \theta < 3\varphi/4$ could be conservatively taken as the UDR. Correspondingly, the average curvature radius in this region could reasonably be taken as the bending radius. Thus, based on Eq 22, the bending radius is calculated as

$$R = \frac{\int_{\varphi_1}^{\varphi_2} \rho(\theta)d\theta}{\varphi_2 - \varphi_1} = \frac{\int_{\varphi_1}^{\varphi_2} \left[2C\int_0^{b(\theta)} y^{n+1}B(\theta,y)dy\right]^{1/n} d\theta}{M^{1/n}(\varphi_2 - \varphi_1)} \quad \text{(Eq 23)}$$

where φ_1 and φ_2 are the boundaries of the UDR; $\rho(\theta)$ is the curvature radius at θ.

Equation 23 yields

$$M = \left\{ \frac{\int_{\varphi_1}^{\varphi_2} \left[C\int_{-b(\theta)}^{b(\theta)} y^{n+1}B(\theta,y)dy\right]^{1/n} d\theta}{R(\varphi_2 - \varphi_1)} \right\}^n \quad \text{(Eq 24)}$$

Substituting Eq 24 into Eq 22, we obtain

$$\begin{aligned}\rho(\theta) &= \left(2C\int_0^{b(\theta)} y^{n+1}B(\theta,y)dy\right)^{1/n} \cdot \frac{R(\varphi_2 - \varphi_1)}{\int_{\varphi_1}^{\varphi_2}\left[2C\int_0^{b(\theta)} y^{n+1}B(\theta,y)dy\right]^{1/n} d\theta} \\ &= \left\{a(\theta)b(\theta)^{n+2} - [a(\theta)-t][b(\theta)-t]^{n+2}\right\}^{1/n} \cdot \frac{R(\varphi_2 - \varphi_1)}{\int_{\varphi_1}^{\varphi_2}\left\{a(\theta)b(\theta)^{n+2} - [a(\theta)-t][b(\theta)-t]^{n+2}\right\}^{1/n} d\theta}\end{aligned} \quad \text{(Eq 25)}$$

To calculate the springback angle, the bent tube is divided into many tube segments with infinitesimally small lengths. Within each small segment, the variation in cross-sectional dimensions is negligible compared with the dimensions of the cross section. Thus, it is feasible to consider each segment (see Fig. 3) as a uniformly distorted one for approximation. Consider the tube segment between θ and $\theta + d\theta$. Its bending angle is $d\theta$; the lengths of the major and minor axes of the distorted cross section are $a(\theta)$ and $b(\theta)$, respectively; the springback angle is denoted as $\Delta(d\theta)$; the curvature radius before loading is $\rho(\theta)$, which is expressed as Eq 25. Therefore, similar to Eq 17, the springback angle could be calculated as

$$\Delta(d\theta) = \frac{16C\left\{a(\theta)b(\theta)^{n+2} - [a(\theta)-t][b(\theta)-t]^{n+2}\right\}^{1/n}\left\{\frac{R(\varphi_2-\varphi_1)}{\int_{\varphi_1}^{\varphi_2}\left\{a(\theta)b(\theta)^{n+2} - [a(\theta)-t][b(\theta)-t]^{n+2}\right\}^{1/n} d\theta}\right\}^{1-n}}{\pi E\left\{a(\theta)b(\theta)^3 - [a(\theta)-t][b(\theta)-t]^3\right\}} \cdot \eta \cdot d\theta \quad \text{(Eq 26)}$$

Integrating this equation alongside the tangential direction, we obtain the springback angle of the whole bent tube:

$$\Delta\varphi = \frac{16\eta CR^{1-n}}{\pi E}\int_0^{\varphi} \frac{\left\{a(\theta)b(\theta)^{n+2} - [a(\theta)-t][b(\theta)-t]^{n+2}\right\}^{1/n}\left\{\frac{(\varphi_2-\varphi_1)}{\int_{\varphi_1}^{\varphi_2}\left\{a(\theta)b(\theta)^{n+2} - [a(\theta)-t][b(\theta)-t]^{n+2}\right\}^{1/n} d\theta}\right\}^{1-n}}{\left\{a(\theta)b(\theta)^3 - [a(\theta)-t][b(\theta)-t]^3\right\}} d\theta \quad \text{(Eq 27)}$$

Based on Eq 25, the tangential strain at the extrados could be calculated as

$$\begin{aligned}\varepsilon_{\max}(\theta) &= \frac{b(\theta)}{\rho(\theta)} \\ &= \frac{b(\theta)\int_{\varphi_1}^{\varphi_2}\left\{a(\theta)b(\theta)^{n+2} - [a(\theta)-t][b(\theta)-t]^{n+2}\right\}^{1/n} d\theta}{\left\{a(\theta)b(\theta)^{n+2} - [a(\theta)-t][b(\theta)-t]^{n+2}\right\}^{1/n} R(\varphi_2-\varphi_1)}\end{aligned} \quad \text{(Eq 28)}$$

The tangential strain at a position other than the extrados could be calculated using Eq 20 and 28.

The integrals in Eq 27 and 28 are calculated though numerical integration utilizing MATLAB. The values of a and b were obtained experimentally.

4. Experiment

The cross-sectional dimensions after bending were obtained through bending tests of tubes. Tubes of 1Cr18Ni9Ti stainless steel and 5A03 aluminum alloy were tested. The mechanical properties of both materials obtained though tensile tests are presented in Table 1.

Bending tests were carried out utilizing a VB-100HP CNC bending machine. Neither axial force nor internal pressure was applied in the tests. Tests with bending angles of 45°, 90°, 145°, and 180° were performed. The lengths of the major and minor axes of the distorted cross sections were measured. Tubes bent to $\varphi = 45°$ or 90° were measured at $\theta = 0$, $\theta = \varphi/2$, and $\theta = \varphi$

while those bent to φ = 145° or 180° were measured at θ = 0, φ/4, φ/2, 3φ/4, and φ. Based on the measured values at these points, the lengths of the major and minor axes of the cross sections at all tangential positions were obtained through cubic spline interpolation. In addition to the cross-sectional dimensions, the springback angles of some bent tubes were measured with a laser measuring instrument.

5. Results and Discussion

5.1 Strain Distribution

The ovalizations of one steel tube and two aluminum tubes obtained through measurements and cubic spline interpolation are shown in Fig. 4. The ovalization is characterized by the ratio of the semi-major axis to the original tube radius (a/r) and the ratio of the semi-minor axis to the original radius (b/r). Based on this result, the maximum tangential strain values both by neglecting ovalization and considering ovalization are calculated utilizing Eq 9 and 28, respectively. Comparison between the two calculations (see Fig. 5) indicates that ovalization leads to a decrease in the maximum tangential strain in both the UDR and the NUDR. Also, as a result of the non-uniformity of ovalization, the tangential deformation is not uniform in the longitudinal direction; the deformation is much less severe in the NUDR than in the UDR. In the UDR, the deformation is basically uniform, but in the NUDR, a gradual variation in the degree of deformation is seen. Furthermore, the ovalization of aluminum tubes is more significant than that of steel tubes. Also, both the reduction in maximum tangential strain and the non-uniformity of deformation are more obvious in the aluminum tubes than in the steel tube.

The non-uniform bending deformation revealed by calculation could be verified by FE simulation and experiments. Figure 6 shows the simulation result of a 1Cr18Ni9Ti stainless steel tube (Ref 19). The thickness strain at the extrados (or intrados) is the greatest in the middle and decreases toward both ends. This means that the deformation is less severe at the ends than in the middle. Furthermore, since it is generally considered that the circumstantial strain is small compared with the tangential strain and the thickness strain, it could be inferred that the distribution of tangential strain is similar with that of thickness strain shown in the figure. This coincides with the calculation considering ovalization. Moreover, the calculation result of tangential strain agrees qualitatively with published experimental results. Al-Qureshi and Russo (Ref 14) divided a bent tube into several segments and measured the tangential strain in each segment. It was found that the tangential strain is the largest in the middle; the nearer to the ends, the smaller the tangential strain.

Table 1 Mechanical properties of tube materials

Material	*E*, GPa	*C*, MPa	*n*
Steel (1Cr18Ni9Ti)	198	1093	0.374
Aluminum (5A03)	73	273	0.160

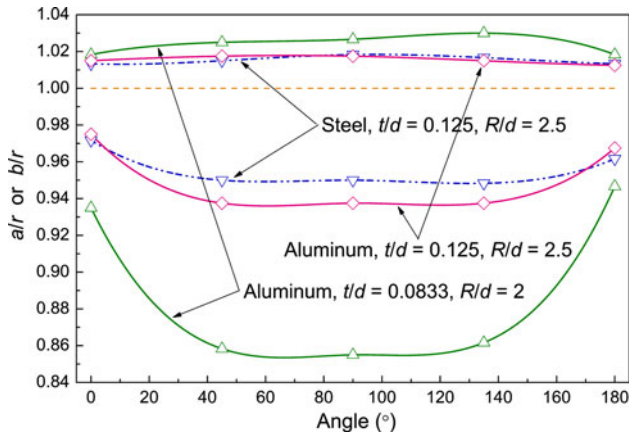

Fig. 4 Distribution of ovalization in the longitudinal direction

5.2 Springback

Taking the cross-sectional ovalization into account results in a larger predicted springback angle as shown in Fig. 7-9. It has been demonstrated that when the bending angle remains constant, the springback angle increases with an increasing

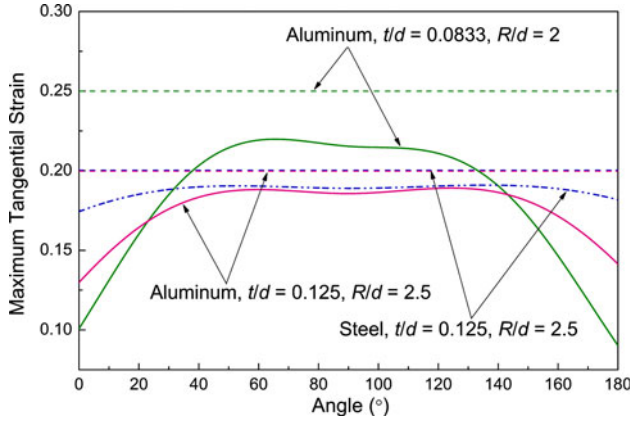

Fig. 5 Distribution of the maximum tangential strain in the longitudinal direction. The straight lines are the calculation results neglecting ovalization; the curves are the calculation results considering ovalization

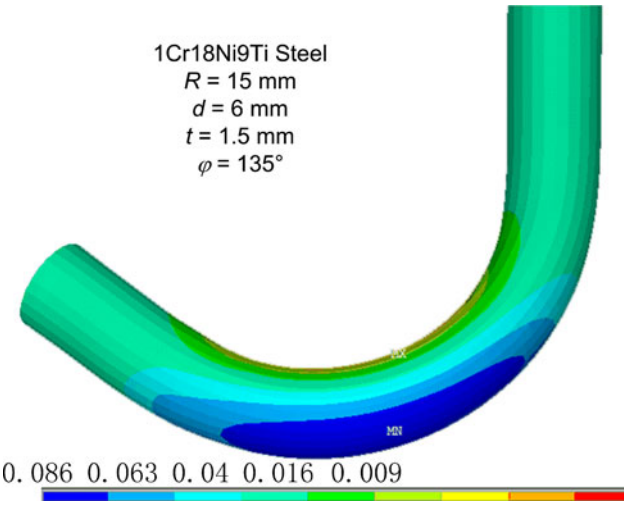

Fig. 6 Simulation result of the thickness strain (Ref 19)

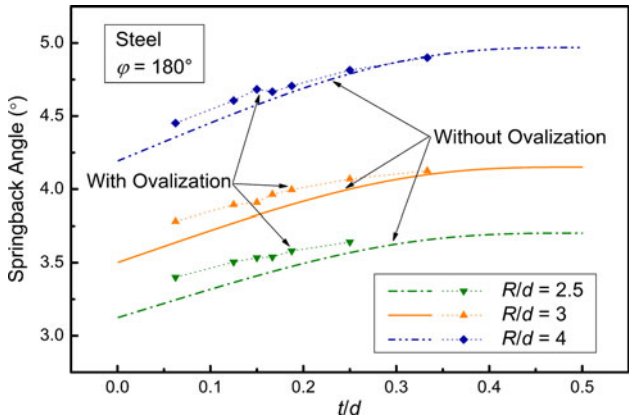

Fig. 7 Calculated springback angles with various wall thickness ratios

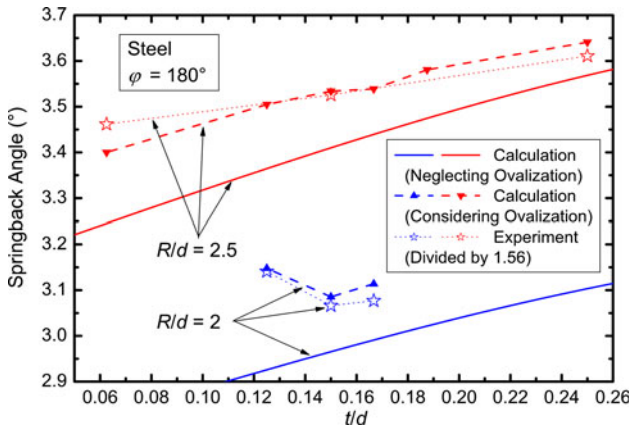

Fig. 8 Theoretical and experimental springback angles with various wall thickness ratios

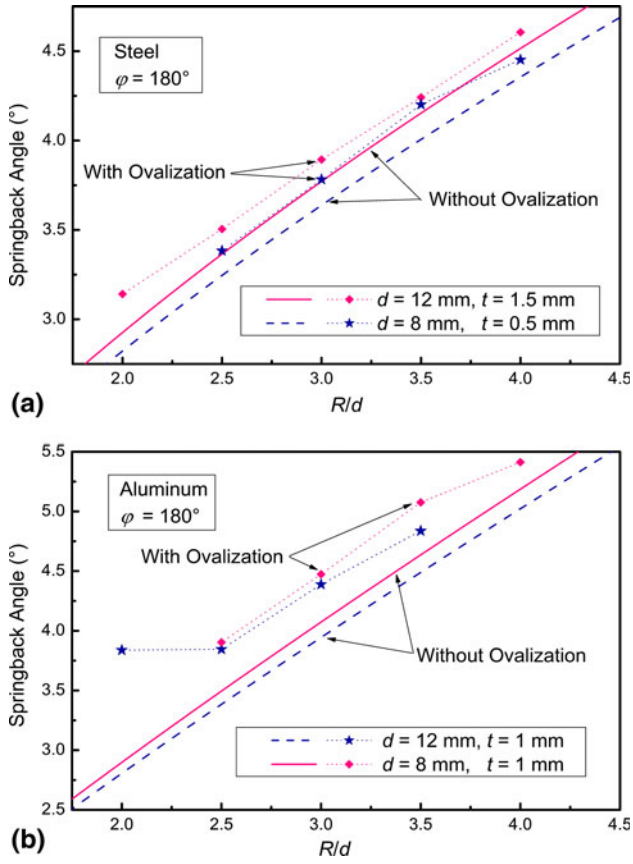

Fig. 9 Calculated springback angles with various bending radius ratios. (a) steel tubes; (b) aluminum tubes

bending radius ratio (Ref 17). Equation 22 indicates that since the distorted cross section is more ovalized in the middle than at the ends, the curvature radius in the NUDR is greater than that in the URD, which is considered as the bending radius. Experiments also show that the curvature radius is not equal in different tube sections. As a result, the actual specific springback angle $\Delta\varphi/\varphi$ in the NUDR is greater than that predicted using the bending radius. Moreover, ovalization reduces the distance between the tube wall and the neutral surface, which means that the effect of ovalization is similar to that of a reduction in tube diameter: both of them reduce the tangential strain, raise the portion of elastic deformation, and thus increase the magnitude of springback (Ref 17).

To evaluate the degree to which the springback angle is raised, a parameter D is introduced:

$$D = \frac{\Delta\varphi_{\mathrm{Oval}} - \Delta\varphi_{\mathrm{Circ}}}{\Delta\varphi_{\mathrm{Circ}}} \times 100\% \qquad \text{(Eq 29)}$$

where $\Delta\varphi_{\mathrm{Oval}}$ and $\Delta\varphi_{\mathrm{Circ}}$ are the predicted springback angles by considering ovalization (Eq 27) and neglecting ovalization (Eq 7), respectively. D will be referred to as the "calculation deviation rate" in the following discussions.

In tube bending, the springback angle is determined by material parameters (including C, E, and n) and geometrical parameters (the bending angle φ, the outer diameter d, the wall thickness t, and the bending radius R). Without considering the size effect (Ref 20), the springback angles of tubes of the same material and bending angle are equal only if the R:d:t ratios are the same. That is to say, there are only three independent geometrical parameters: bending angle φ, wall thickness ratio t/d, and bending radius ratio R/d. In this section, the effects of these three parameters on D will be discussed. The effects of material properties will also be addressed by comparing the aluminum tubes with the steel tubes.

Table 2 Calculation deviation rates with different bending angles

	D, %			
Material	**45°**	**90°**	**135°**	**180°**
Steel	4.3	7.4	8.6	7.6
Aluminum	46.7	36.2	37.4	35.4

5.2.1 Bending Angle. Bending angle does not have a significant effect on the calculation deviation rate. Table 2 shows that the D value is basically the same for different bending angles (except 45°). What is more, the two tubes in the table have similar geometrical parameters, but the D values of the aluminum tube are much larger than those of the steel tube. The ovalization of the steel tube is negligible for approximate calculation while the ovalization of the aluminum tube must be

Table 3 Calculation deviation rates of steel tubes with various wall thickness ratios (R/d = 3)

t/d	0.0625	0.125	0.15	0.1667	0.1875	0.25	0.3333
$(d-b)/d$, %	6.15	3.99	3.57	4.15	3.11	0.99	0.58
D, %	4.0	3.2	2.3	2.8	2.6	1.7	0.7

Table 4 Ovality and calculation deviation rates of aluminum tubes with various bending radius ratios

R/d	2	2.5	3	3.5
$(r-b)/r$, %	14.58	9.02	8.18	4.36
D, %	36.8	13.6	11.3	7.7

considered. That is to say, whether ovalization is negligible is considered on a case-to-case basis; it depends largely on the mechanical property of the tube material.

5.2.2 Wall Thickness Ratio. The springback angle increases as the wall thickness ratio increases as shown in Fig. 7. According to the calculation in Ref 17, the springback angle increases first and reduces afterward with the increase of t/d. Obviously, the monotonic relation is more realistic.

If ovalization is taken into consideration, it results in larger predicted springback angles for all the wall thickness ratios. Table 3 shows that as t/d increases, the ovality reduces. The influence of ovalization on springback also becomes less significant; it becomes very insignificant when t/d reaches 1/3. Moreover, the smaller the R/d, the more significant the influence of ovalization on springback. When $R/d \geq 2.5$ (see Fig. 7), the predicted springback angle considering ovalization increases with the increase of t/d, though the slope is smaller than its counterpart when neglecting ovalization. However, in the case of $R/d = 2$ (see Fig. 8), the trend of springback angle over wall thickness ratio has been changed by the pronounced ovalization. The experimental data in Fig. 8 indicate that considering ovalization renders a more accurate prediction of the trend of springback over t/d. The experimental results have been divided by a factor (1.56 for this specific material and bending process) so that they could be better compared with the calculations. Therefore, the analytic results could be well applied to production after proper correction. As for the quantitative discrepancy between experimental and analytical results, it is mainly due to an undesirable deformation of the straight portion of the tube (Ref 16, 17).

5.2.3 Bending Radius Ratio. The severity of ovalization is a function of the bending radius ratio. Table 4 presents the ovality (characterized by $(r-b)/r$, the rate of change of the minor axis) at the mid span and the consequential calculation deviation rates. Clearly, with a decreasing R/d, the bending deformation becomes more severe, and the ovality thus increases. The D values also increase, which means that the discrepancy between the calculations considering ovalization and that neglecting ovalization becomes larger (see Fig. 9). That is to say, R/d influences the calculation deviation rate indirectly through affecting the degree of ovalization. However, it should be noted that even if both the dimensions and the degree of ovalization of two bent tubes are the same, their D values are usually different if their materials are different. Actually, in Eq 7 and 27, n exists in the integral terms that incorporate the major and minor axes and thus has an effect on D while C and E do not influence the D value directly.

Table 5 Experimental springback angles with small bending radius ratios

R/d	Δφ, °
2	3.2
2.5	3.3

The tubes are aluminum ones with t/d = 0.0833 bent to 180°

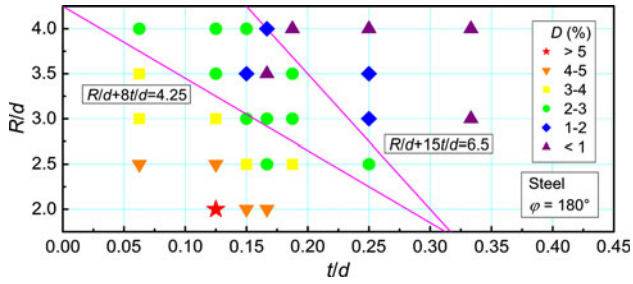

Fig. 10 Calculated deviation rates of steel tubes

Figure 9 shows the calculated springback angles of aluminum tubes and steel tubes. Within the range of R/d shown in the figure, the predicted springback angle neglecting ovalization increases almost linearly with the increase of R/d. For the steel tubes, there is a slight influence of ovalization on springback, and the shape of the curve has been changed little. However, for aluminum tubes, taking ovalization into account has resulted in a marked change. When R/d is small enough (less than 2.5), the increment in predicted springback angle caused by considering ovalization will offset the reduction caused by the decrease of R/d. Thus, the calculation result of $R/d = 2$ is almost the same with that of $R/d = 2.5$, which is verified by experiments (see Table 5).

5.2.4 The Condition on Which Ovalization is Negligible. The discussions above show that the bending angle does not have a significant effect on the calculation deviation rate; instead, the material properties, bending radius ratio, and wall thickness ratio are found to be the most influential factors. For each tube material, the limit condition on which the effect of ovalization on springback is negligible is obtained empirically as shown in Fig. 10. Utilizing different colors, the calculation deviation rates corresponding to various R/d and t/d values are shown. When $R/d + 8t/d > 4.25$, the calculation deviation rate is less than 3%. When $R/d + 15t/d > 6.5$, the rate is less than 2%. The limit condition of other materials could also be obtained in the same way. This method could be useful in designing and engineering calculation.

6. Conclusions

In this study, a model considering non-uniform ovalization has been developed to calculate the springback angle and tangential strain in tube bending. Through comparing the calculation results by considering ovalization and those by neglecting ovalization with experimental data, it is shown that the proposed model is more accurate. The qualitative correlation between springback angle and geometrical parameters (R/d and t/d) shown in experiments could be better predicted

using the model considering springback. After simple correction, the predicted values could be well applied to practical bending processes.

Taking ovalization into account leads to a larger predicted value of springback. The inaccuracy caused by neglecting ovalization various greatly with bending radius ratio and wall thickness ratio. The smaller the R/d and t/d the values, the more significant the influence of ovalization on springback. Moreover, the influence of ovalization differs a lot from one material to another. The ovalization of the aluminum tubes is much more influential than that of the steel tubes. For aluminum tubes with relatively small R/d and t/d values, ovalization must be considered to obtain a precise calculation.

The effects of ovalization on strain distribution have also been explored. Calculation indicates that ovalization leads to a reduction in the maximum tangential strain. Moreover, non-uniform ovalization results in non-uniform deformation; the bending deformation is the most severe in the middle segment of the bent tube.

The authors believe that this research could facilitate future explorations into the bending deformation of tubes. Though only circular tubes have been dealt with in this article, cross sections with other shapes could also be studied with a similar approach. It is also believed that the results of strain distribution will be helpful in investigating springback as well as other defects in tube bending.

References

1. J.E. Miller, S. Kyriakides, and A.H. Bastard, On Bend-Stretch Forming of Aluminum Extruded Tubes. I. Experiments, *Int. J. Mech. Sci.*, 2001, **43**, p 1283–1317
2. L.G. Brazier, On the Effect of Flexure of Thin Cylindrical Shells and Other Thin Sections, *Proc. R. Soc. Lond. Ser. A*, 1927, **116**, p 104–114
3. H. Zhu and K.A. Stelson, Distortion of Rectangular Tubes in Stretch Bending, *J. Manuf. Sci. Eng. (Trans. ASME)*, 2002, **124**, p 886–890
4. K.A. Stelson and A. Kramer, Distortion of U-Channel Sections in Plastic Bending, *J. Manuf. Sci. Eng. (Trans. ASME)*, 1999, **121**, p 208–213
5. F. Paulsen and T. Welo, Cross Sectional Deformations of Rectangular Hollow Sections in Bending. Part I. Experiments, *Int. J. Mech. Sci.*, 2001, **43**, p 109–129
6. J.E. Miller, S. Kyriakides, and E. Corona, On Bend-Stretch Forming of Aluminum Extruded Tubes. II. Analysis, *Int. J. Mech. Sci.*, 2001, **43**, p 1319–1338
7. S. Kyriakides, E. Corona, and J.E. Miller, Effect of Yield Surface Evolution on Bending Induced Cross Sectional Deformation of Thin-Walled Sections, *Int. J. Plast.*, 2004, **20**, p 607–618
8. J. Wang and A. Agarwal, Tube Bending Under Axial Force and Internal Pressure, *J. Manuf. Sci. Eng. (Trans. ASME)*, 2006, **128**, p 598–605
9. N.C. Tang, Plastic-Deformation Analysis in Tube Bending, *Int. J. Pressure Vessels Piping*, 2000, **77**, p 751–759
10. M. Elchalakani, X.L. Zhao, and R.H. Grzebieta, Plastic Mechanism Analysis of Circular Tubes Under Pure Bending, *Int. J. Mech. Sci.*, 2002, **44**, p 1117–1143
11. H. Naoi, N. Kitakami, M. Mizumura, and Y. Kuriyama, Study of Intrusion Bending for Steel Tubes with Thin Wall Thickness, *J. Mater. Eng. Perform.*, 2008, **17**, p 376–381
12. D. Tang, D. Li, Z. Yin, and Y. Peng, Roles of Surface Booster System on Bending of Thin-Walled Copper Tube, *J. Mater. Eng. Perform.*, 2009, **18**, p 369–377
13. H.A. Al-Qureshi, Elastic-Plastic Analysis of Tube Bending, *Int. J. Mach. Tools Manuf.*, 1999, **39**, p 87–104
14. H.A. Al-Qureshi and A. Russo, Spring-Back and Residual Stresses in Bending of Thin-Walled Aluminium Tubes, *Mater. Des.*, 2002, **23**, p 217–222
15. A. Megharbel, G.A. Nasser, and A. Domiaty, Bending of Tube and Section Made of Strain-Hardening Materials, *J. Mater. Process. Technol.*, 2008, **203**, p 372–380
16. M. Zhan, H. Yang, L. Huang, and R. Gu, Springback Analysis of Numerical Control Bending of Thin-Walled Tube Using Numerical-Analytic Method, *J. Mater. Process. Technol.*, 2006, **177**, p 197–201
17. D. E and Y. Liu, Springback and Time-Dependent Springback of 1Cr18Ni9Ti Stainless Steel Tubes under Bending, *Mater. Des.*, 2010, **31**, p 1256–1261
18. G. Khodayari, How Material Influences Bending for Hydroforming: Effects on Ovality, Springback, and Wall Thickness in Tubes, *Tube Pipe J.*, 2002
19. D. E, R. Ning, and T. Gu, Experiment and Analysis on the Distortion of Cross Section of Bended-Tube, *Acta Armamentarii*, 2006, **27**, p 698–701 (in Chinese)
20. T. Fülöp, W.A.M. Brekelmans, and M.G.D. Geers, Size Effects from Grain Statistics in Ultra-Thin Metal Sheets, *J. Mater. Process. Technol.*, 2006, **174**, p 233–238